Dephasing of Stark wave packets induced by colored noise

S. Yoshida,[1] C. O. Reinhold,[2,3] J. Burgdörfer,[1,3] W. Zhao,[4] J. J. Mestayer,[4] J. C. Lancaster,[4] and F. B. Dunning[4]
[1]*Institute for Theoretical Physics, Vienna University of Technology, Vienna, Austria, EU*
[2]*Physics Division, Oak Ridge National Laboratory, Oak Ridge, Tennessee 37831-6372, USA*
[3]*Department of Physics, University of Tennessee, Knoxville, Tennessee 37996, USA*
[4]*Department of Physics and Astronomy and the Rice Quantum Institute, Rice University, Houston, Texas 77005-1892, USA*
(Received 1 August 2006; published 17 January 2007)

The time evolution of Stark wave packets in Rydberg atoms under the influence of colored noise is analyzed. The Stark wave packets are generated by exposing $K(350p)$ Rydberg atoms to an electric field step. Their time evolution is monitored using a half-cycle probe pulse that is applied after a variable time delay. The noise is generated by randomly modulating the amplitude of the static field. We show that noise results in an enhanced and irreversible dephasing of Stark quantum beats, as monitored by the damping of the beat amplitude. This source of decoherence is most effective when the characteristic frequency of the noise power spectrum matches the orbital frequency of the Rydberg electron. Noise driven resonant $\Delta n=1$ transitions broaden the energy distribution thereby accelerating the dephasing.

DOI: 10.1103/PhysRevA.75.013414 PACS number(s): 32.80.Rm, 32.60.+i

I. INTRODUCTION

A coherent superposition of nondegenerate quantum states localized in space is called a wave packet [1]. Recent advances in ultra-short pulse generation allow wave packets in Rydberg atoms to be engineered [2–4] and have stimulated the investigation of possible protocols to manipulate their dynamics [5–8]. Such studies of Rydberg wave packets promise applications in many areas of physics, such as quantum information [9,10] and control of chemical reactions [11]. Moreover, Rydberg wave packets are a very useful tool for understanding the crossover between classical and quantum dynamics because their behavior frequently mirrors the dynamics of the corresponding classical system.

The ubiquitous coupling of a microsystem to its environment, i.e., to noise, tends to destroy the coherent superposition by randomly dephasing the different components of the wave packet relative to one another. This source of decoherence provides a fundamental limitation to coherent quantum manipulation and quantum information processing. Decoherence induced by dephasing converts a coherent superposition into a incoherent statistical mixture and is, therefore, often invoked in facilitating the quantum-to-classical transition of microscopic and mesoscopic dynamics [12–16].

Rydberg atoms are of particular interest in the study of decoherence. Apart from possible applications to quantum information processing [9,10], they provide a powerful probe of the quantum-to-classical transition [17,18] because of their quasi-classical behavior for large quantum numbers, even in the absence of noise. As the principal quantum number n increases, the Heisenberg time (or quantum break time) where classical and quantum dynamics diverge, $\tau_H \propto n^4$, can reach times of the order of a microsecond (for $n=350$). One signature of quantum behavior is the revival of Rydberg wave packets [19–22], which is absent in classical dynamics. Since Rydberg atoms are fragile and are highly susceptible to environmental interactions, dephasing and decoherence can proceed on a short time scale. More precisely, the dephasing (or decoherence) time τ_D can be shorter than τ_H. In this case, decoherence will not only eventually render a quantum system classical but will strongly modify the quantum evolution at a stage where it still closely follows the classical evolution. Stark quantum beats that have a classical counterpart are the case in point. For $\tau_D < \tau_H$, Stark beats are damped due to the dephasing of different components of the coherent superposition. This dephasing, which occurs in the absence of noise, is referred to in the following as coherent dephasing. It maintains coherence and is reversible. Revivals are one hallmark of this reversibility. Noise induced dephasing, on the other hand, induces an additional damping that is irreversible and signifies decoherence. We investigate in the following noise induced dephasing and damping of quantum (or classical) beats in Stark wave packets. The present system allows experimental and theoretical study of the influence of decohering interactions on short time scales, $t < \tau_H$. Moreover, it is possible to electronically synthesize in a controlled manner colored (rather than "white") noise with a spectral distribution that matches characteristic frequencies of the system. (The properties of the colored noise used in this study are discussed in more detail in Sec. III.) We investigate the dependence of the dephasing on frequency and amplitude of noise. Atomic units are used unless otherwise indicated.

II. STARK WAVE PACKETS IN HIGH RYDBERG STATES

A Stark wave packet comprising a coherent superposition of several parabolic states can be created by exciting atoms with a short laser pulse in a static dc electric field F_{dc} [2] or by suddenly exposing highly-excited Rydberg atoms (typically in np states) to a dc field [23,24]. In the weak field regime where different n-manifolds are well separated, the energy levels of hydrogenic parabolic states are given by

$$E_{nk} = -\frac{1}{2n^2} + \frac{3}{2}nkF_{dc}, \tag{1}$$

where F_{dc} is the applied dc field and n and k are the principal and electric quantum numbers, respectively [25]. In the fol-

lowing all electric fields are applied along the z-axis of quantization and, therefore, the magnetic quantum number $m=0$ is conserved.

The Stark wave packet created by the field step can be written as a coherent superposition of parabolic states,

$$|\psi(t)\rangle = \sum_{n,k} c_{nk} e^{-iE_{nk}t} |nk\rangle, \tag{2}$$

where $|nk\rangle$ is the parabolic state, E_{nk} is its eigenenergy [approximated to first order by Eq. (1)]. The time evolution of the wave packet is governed by energy differences between parabolic states and resembles, for fixed n, that of the well-known coherent states of the harmonic oscillator [26,27], i.e.,

$$E_{nk'} - E_{nk} \simeq \omega_s(n)(k'-k)/2 = \omega_s \delta k/2, \tag{3}$$

which corresponds to an integer multiple of the Stark precession frequency $\omega_s(n)=3nF_{\mathrm{dc}}$. Note that δk for fixed n is even since $k=-(n-|m|-1),-(n-|m|-1)+2,\ldots,n-|m|-1$.

The expansion coefficients $c_{nk}=\langle nk|\psi(t=0)\rangle$ are the projection amplitudes of the initial stationary Rydberg state onto Stark states when F_{dc} is suddenly turned on. In the experiment discussed in the following $|\psi(t=0)\rangle$ is the laser excited 350p. For sufficiently strong F_{dc}, Stark manifolds originating from different n overlap and the coherent superposition [Eq. (2)] includes several n levels introducing additional beat frequencies. The spacing between levels in adjacent Rydberg manifolds is approximately harmonic oscillator like. Specifically, for $n'-n=\delta n \ll n$ and $k'-k=\delta k \ll n$

$$E_{n'k'} - E_{nk} \simeq \omega_n(k)\,\delta n + \frac{\omega_s(n)}{2}\delta k, \tag{4}$$

where

$$\omega_n = \omega_n^0 + \frac{3}{2}kF_{\mathrm{dc}} \tag{5}$$

and $\omega_n^0=1/n^3$ is the field-free classical Kepler frequency [$\omega_n(k)\to\omega_n^0$ in the limit $F_{\mathrm{dc}}\to 0$]. Equation (3) is seemingly a particular case of Eq. (4) [note that δn and δk in Eq. (3) must be either both odd and both even]. However, Eq. (4) is a first order expansion whereas Eq. (3) is valid to all orders irrespective of the condition $\delta k \ll n$.

The key point for classical-quantum correspondence is that both ω_n and ω_s are directly related to the classical frequencies of the angle variables of the action-angle representation of the classical Hamiltonian. Equation (1) corresponds approximately to the Hamiltonian in action-angle variables (n,k,θ_n,θ_k) where θ_n and θ_k are the angles corresponding to the classical actions n and k, respectively (for a detailed discussion of the Stark problem in action-angle variables see Refs. [28–31]). Using Hamilton's equations of motion, the frequency ω_n is identified as the angular velocity of θ_n, i.e., $\omega_n=|d\theta_n/dt|=|\partial E_{nk}/\partial n|$. In turn, $\omega_s/2$ is the angular velocity of θ_k, i.e., $\omega_s/2=\omega_k=|d\theta_k/dt|=|\partial E_{nk}/\partial k|$. The quantum beat frequencies of Eq. (4) are therefore multiples of the classical beat frequencies. A coherently excited wave packet has a direct analogue in terms of an oscillatory motion in classical phase space, evolving dispersion free similar to a harmonic oscillator. In a weak field F_{dc} different n-manifolds are well separated and a Stark wave packet can be created within a single n-manifold. Therefore its time evolution is governed by the energy separation $\omega_s(n)$ and its higher harmonics [Eq. (3)]. As these are equispaced in energy, the wave packet evolves without dispersion. In stronger fields the Stark manifolds for different n overlap and mixing occurs. The different frequencies $\omega_s(n)$ for the different n-manifolds lead to coherent dephasing and damp the periodic motion associated with Stark precession, i.e., the Stark beats. The periodic motion associated with Kepler orbits also dephases because the energy separations yielding $\omega_n(k)$ are not constant when the higher order terms in the Taylor expansion are included. The beats due to Stark precession and Kepler orbital motion damp faster as the n-distribution becomes broader. The presence of different discrete frequencies for various δk and δn lead to dephasing of the quantum wave packet of an isolated atom that is, however, reversible and maintains its coherence. After a certain time, the different frequency components can rephase leading to (fractional) revival of the periodic behavior [20–22]. The dephasing induced by the spread of the discrete frequency spectrum does not erase the quantum coherence of the wave packet. In contrast, in classical dynamics, n and k are continuously distributed leading thus to a loss of classical coherence, i.e., to dephasing without any revivals. The time scale for partial revival and, thus, for breakdown of classical-quantum correspondence defines the Heisenberg time τ_{H} in this system. The present noise-induced dephasing and thus damping of Stark beats, however, occurs on a time scale $t \ll \tau_{\mathrm{H}}$. In this short-time regime, which for the present system ($n=350$) extends to times approaching a microsecond, classical and quantum coherence are equivalent. (Revival times are too long to be observed in the present experimental set-up.) We study in the following this short time regime in which the coherent classical (or quantum) dephasing can be modified by noise induced decoherence on a time scale $\tau_{\mathrm{D}} < \tau_{\mathrm{H}}$, and investigate the effect of colored noise.

III. SIMULATION OF DYNAMICS IN THE PRESENCE OF NOISE

The short-time dynamics of wave packets can be simulated using the classical trajectory Monte Carlo (CTMC) method. The restricted microcanonical ensemble ($n=350, l=1$) of points in phase space that represents the initial p-state is propagated in time according to Hamilton's equation of motion for the hydrogenic Hamiltonian

$$H(t) = H_{\mathrm{at}} + V(t) \tag{6}$$

with

$$H_{\mathrm{at}} = \frac{p^2}{2} - \frac{1}{r}, \quad V(t) = zF(t) \tag{7}$$

where $\vec{r}=(x,y,z)$ and $\vec{p}=(p_x,p_y,p_z)$ are the position and momentum of the electron, respectively. We consider now the coupling of the atomic system [Eq. (6)] to its environment. This coupling to environmental degrees of freedom can be approximated through a stochastic interaction, so-called

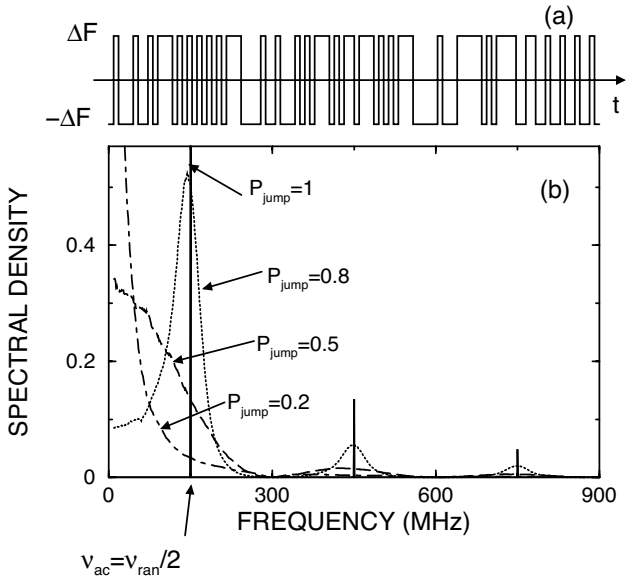

FIG. 1. (a) Typical noise signal $F_{\mathrm{ran}}(t)$ as a function of time. (b) Spectral densities of the noise associated with different values of P_{jump} (see text). $\nu_{\mathrm{ran}}=300$ MHz.

noise. We will simulate colored noise whose spectral density is not distributed uniformly in frequency and explore the influence of its characteristic distribution frequency on the decoherence, i.e., the irreversible damping of Stark beats. To approximate the experimentally generated noise signal, the applied field $F(t)$ is decomposed into two parts

$$F(t) = F_{\mathrm{dc}} + F_{\mathrm{ran}}(t) \tag{8}$$

where the dc field F_{dc} determines the period of the Stark beats and the random component $F_{\mathrm{ran}}(t)$ introduces stochastic variations and thus dephasing. $F_{\mathrm{ran}}(t)$ is realized by a binary-valued random sequence

$$F_{\mathrm{ran}}(t) = \sum_{j\geqslant 1} F_j \chi_j^{T_{\mathrm{ran}}}(t) \tag{9}$$

where

$$F_j = \pm \Delta F \tag{10}$$

and $\chi_j^{T_{\mathrm{ran}}}(t)$ is the characteristic function of the interval $[(j-1)T_{\mathrm{ran}}, jT_{\mathrm{ran}}]$. As illustrated in Fig. 1(a), $F_{\mathrm{ran}}(t)$ discontinuously jumps randomly between these two values of F_j after fixed time intervals T_{ran} and remains constant $F_{\mathrm{ran}}(t)=F_j$ during each interval $(j-1)T_{\mathrm{ran}}<t<jT_{\mathrm{ran}}$. (The corresponding frequency is $\nu_{\mathrm{ran}}=1/T_{\mathrm{ran}}$.) Differently colored noise can be generated by choosing different probability functions for the jumps between $+\Delta F$ and $-\Delta F$. We introduce the jump probability for reversing the sign of F_j at the jump time $t_j = jT_{\mathrm{ran}}$

$$P_{\mathrm{jump}} = P(F_{j+1} = -F_j). \tag{11}$$

Two limiting cases of Eq. (11) are of particular interest. If $P_{\mathrm{jump}}=1$, the noise field becomes a deterministic alternating field with period

$$T_{\mathrm{ac}} = 2T_{\mathrm{ran}} \tag{12}$$

and frequency $\nu_{\mathrm{ac}}=\nu_{\mathrm{ran}}/2$. Maximum randomness is reached for $P_{\mathrm{jump}}=0.5$. Finally, in the limit $P_{\mathrm{jump}}\to 0$, the noise field reduces to an additional dc field. The noise generator used in the experiment features $P_{\mathrm{jump}}=0.5$.

The noise generated by the perturbation [Eqs. (9) and (11)] can be characterized by its power spectrum,

$$I(\nu) = \lim_{N\to\infty} \frac{1}{N} \sum_{\eta=1}^{N} \left| \int F_{\mathrm{ran}}^{\eta}(t) e^{-2\pi i \nu t} dt \right|^2, \tag{13}$$

where N is the number of stochastic realizations of $F_{\mathrm{ran}}^{\eta}(t)$. Figure 1 displays the power spectrum of differently colored noise for $\nu_{\mathrm{ran}}=300$ MHz. The frequency spectrum of $I(\nu)$ must be compared with the characteristic frequencies $\nu_n[=\omega_n/(2\pi)]$ and $\nu_s[=\omega_s/(2\pi)]$ of the beats. Clearly, interesting dynamical effects are to be expected when the spectral density near these characteristic frequencies $I(\nu_n)$ or $I(\nu_s)$ is large. Note that high frequencies beyond ν_{ran} are present due to the discontinuous jumps in $F_{\mathrm{ran}}(t)$.

IV. EXPERIMENT

The present apparatus is described in more detail elsewhere [23]. High-n atoms are created by photo-exciting potassium atoms contained in a thermal-energy beam to a selected np state with $n=350$, $m=0$ using an extra-cavity doubled CR699-21 Rh6G dye laser. Excitation occurs near the center of an interaction region bounded by three pairs of large copper electrodes. Stray fields in the experimental volume can be reduced to 50 μV cm^{-1} by application of small bias potentials to these electrodes [32]. After excitation, a rectangular voltage pulse of 1 μs duration with a rise time of 0.3 ns is applied to a nearby electrode mounted, together with a 50 Ω terminating resistor, on the end of a section of semi-rigid coaxial cable. This pulse establishes a dc field F_{dc} in the experimental volume. However, because the zero baseline voltage associated with the pulse generator drifts in time, its output is ac coupled to the electrode, the small bias required to zero the stray field being provided by a resistive divider. In consequence, the amplitude of the dc field F_{dc} decreases by $\sim$10% over the $\sim$1 μs period that it is applied. The output signal from a (gated) random pulse generator is superposed on the dc field. This generator divides time into a series of bins of widths T_{ran} and in each randomly assigns an output of 0 or 5 V. This output is then attenuated leading to the pulse train illustrated in Fig. 1(a). The time evolution of the Stark wave packet with (and without) noise present is examined using a probe half-cycle pulse (HCP) of duration $T_p\sim 0.6$ ns full width at half maximum that is applied following a variable time delay τ_{delay}. Since the duration is much smaller than the electron orbital period, the probe behaves like an impulse or kick

$$F_{\mathrm{probe}}(t) = -\Delta p_{\mathrm{probe}} \delta(t - \tau_{\mathrm{delay}}). \tag{14}$$

The number of Rydberg atoms remaining in the experimental volume after application of the HCP is determined by field ionization [4]. Measurements with no pulsed fields applied

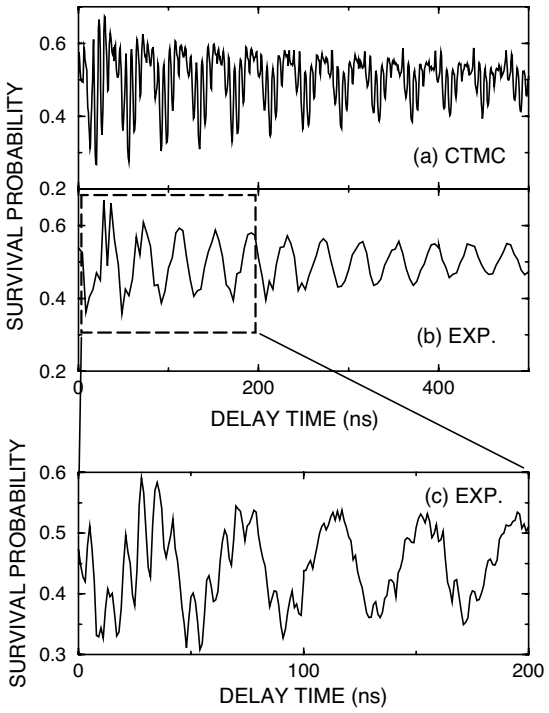

FIG. 2. Time dependence of the survival probability for $K(350p)$ atoms and $F_{dc}=18.8$ mV/cm, $\Delta F=0$, and $\Delta p_{probe}=-0.532/n$ (a.u.) (see text). (a) CTMC simulation, (b) experiment, and (c) magnification of (b) with higher resolution in time.

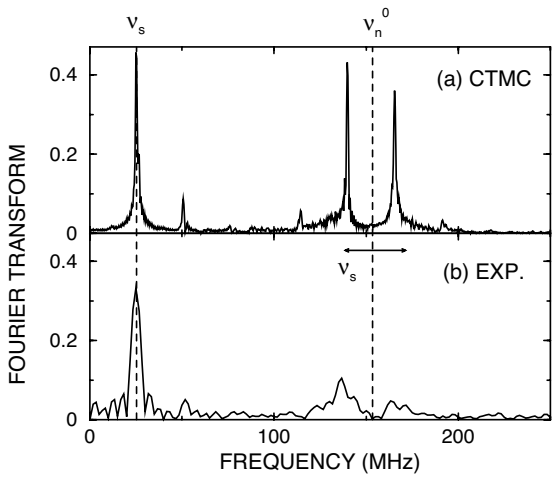

FIG. 3. Fourier transform of the survival probability in Fig. 2 after subtraction of the time-averaged survival probability. (a) CTMC simulation and (b) experiment.

are interspersed at routine intervals during data acquisition to monitor the number of Rydberg atoms initially created by the laser. The Rydberg atom survival probability is determined by taking the ratio of the Rydberg atom signals observed with and without pulse application.

V. DEPHASING OF STARK BEATS

In order to determine the noise-induced dephasing of Stark beats, it is important to first establish the damping due to coherent dephasing as a point of reference. Figure 2 shows measured survival probabilities for the case $\Delta F=0$, i.e., without noise, as a function of the time delay τ_{delay} before application of the probe HCP. High frequency oscillations are evident in the simulations [Fig. 2(a)] as well as in the experimental data [Fig. 2(c)] approximately corresponding to the Kepler frequency ν_n^0 together with slow oscillations [Figs. 2(a) and 2(b)] with the Stark precession frequency ν_s. The field strength F_{dc} used in the measurement is ~ 18.8 mV/cm and is in the strong field regime. Thus, parabolic states with a range of n are excited leading to damping of both the fast and slow oscillations as τ_{delay} is increased.

To quantify the dephasing we calculate the Fourier transform of the survival probability

$$\tilde{P}_s(\nu)=\sqrt{\frac{1}{T}}\int_0^T [P_s(\tau_{delay})-\langle P_s\rangle_\tau]e^{-i2\pi\nu\tau_{delay}}d\tau_{delay}, \tag{15}$$

where the time averaged survival probability $\langle P_s\rangle_\tau$ is subtracted from $P_s(\tau_{delay})$ before the Fourier transform is performed to emphasize the oscillatory behavior. The measured and calculated Fourier transforms in Fig. 3 show two peaks near the Kepler frequency ν_n^0 separated by the Stark frequency ν_s. This is a manifestation of the angular velocities $\nu_n(k)$ in Eq. (4). Since the initial state is a p-state, the present wave packet involves a broad range of k values in the range $-n\lesssim k\lesssim n$. The figure indicates that the dominant frequencies are associated with the extreme values of k: i.e., $\nu_n(k=-n)=\nu_n^0-\nu_s/2$ and $\nu_n(k=n)=\nu_n^0+\nu_s/2$. The reason why the extreme parabolic states dominate in the frequency spectrum is that these states yield the largest variation of the z component of the electron momentum, which is the variable "measured" by the probe pulse. Calculations for a transverse probe (not shown) indicates the complementary result that the Fourier transform has a single high-frequency peak at $\nu_n(k=0)=\nu_n^0$. This peak at $\nu_n(k=0)$ is, however, very small compared to the peaks at $\nu_n(k=\pm n)$ indicating that the electron trajectories are dominated by the motion along the polarization axis defined by F_{dc}.

As expected, the most prominent peak in Fig. 3 is observed around the Stark frequency ν_s. The width of the Fourier peak at ν_s is a direct measure of the damping rate (including the inevitable broadening due to field inhomogeneities in the apparatus and the "droop" in the applied field F_{dc}). The width of the quantum Stark frequency spectrum $\nu_s(n)$ leads to the reversible damping and revival of quantum beats. While quantum mechanically, the peak around ν_s should consist of a set of discrete peaks in the absence of noise, classically it represents a true continuum with nearly the same overall envelope with width $\Delta\nu_{coh}$ such that the initial dephasing time agrees with its quantum mechanical counterpart.

We turn now to the decoherent irreversible damping of Stark beats due to the presence of the colored noise shown in Fig. 1. To this end we study changes of the width of the peak in the Fourier spectrum near ν_s which is approximately the inverse of the decoherence rate $\tau_D^{-1}=\Delta\nu_s$. We note that the decoherence rate corresponds to only the irreversible part of the broadening $\Delta\nu_s-\Delta\nu_{coh}$, but for simplicity we neglect the

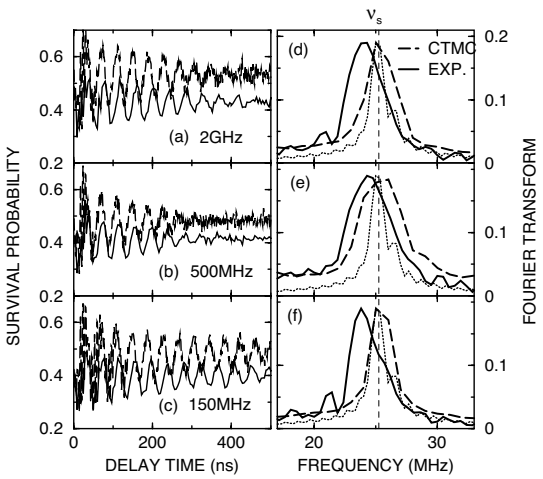

FIG. 4. Measured (solid line) and calculated (dashed line) survival probabilities (left frames) and their Fourier transforms (right frames) in the presence of noise for $F_{dc}=18.8$ mV/cm, $P_{jump}=0.5$, and $\Delta F=0.1F_{dc}$. (a) and (d) $\nu_{ran}=2$ GHz, (b) and (e) $\nu_{ran}=500$ MHz, (c) and (f) $\nu_{ran}=150$ MHz. For comparison, the Fourier spectrum without applied noise is shown by the dotted line. In (d)–(f) the Fourier spectra are renormalized so that all three results have the same peak height.

constant part $\Delta\nu_{coh}$ and study the qualitative response to the applied noise. Measured survival probabilities are shown in Fig. 4 for random noise ($P_{jump}=0.5$) and $T_{ran}=0.5$, 2, and 6.6 ns corresponding to $\nu_{ran}=2$ GHz, 500 MHz, and 150 MHz, respectively, and a noise amplitude, $\Delta F=0.1F_{dc}$. In each case the Stark beats damp faster than in the absence of noise, this being most pronounced for $\nu_{ran}=500$ MHz. Figure 4 also includes the results of CTMC simulations and the Fourier transform of both the theoretical and experimental data. For $\nu_{ran}=500$ MHz the peak near the Stark frequency $\nu_s=25.3$ MHz becomes noticeably broader. Small uncertainties in the amplitude of the applied field F_{dc} (associated with ac coupling and the droop noted earlier) account for the differences in beat frequency evident in Fig. 4. We quantify the peak width in terms of the second moment

$$\tau_D^{-2} \simeq (\Delta\nu_s)^2 = \langle(\nu-\bar{\nu}_s)^2\rangle = \int_{\bar{\nu}_s-\epsilon}^{\bar{\nu}_s+\epsilon} (\nu-\bar{\nu}_s)^2 \tilde{P}_s(\nu)d\nu, \tag{16}$$

where $\bar{\nu}_s \simeq 3nF_{dc}/(2\pi)$ is the average Stark frequency and the integration range, 2ϵ, is chosen to encompass only the peak around the Stark frequency.

Figure 5 displays the measured and calculated widths for various values of $T_{ac}=2T_{ran}$ (in units of the Kepler period $T_n=2\pi n^3=1/\nu_n^0$) and different values of the jump probability, specifically $P_{jump}=1$ (periodic driving), 0.8, and 0.5 (random noise). For $P_{jump}=1$ the response of the Stark wave packet to noise is greatest in narrow ranges centered near

$$\frac{T_{ac}}{T_n} = T_{ac}\nu_n^0 = 2i+1 \tag{17}$$

with $i=0,1,2,\ldots$. Equation (17) implies that the Stark wave packet is resonantly excited by the "noise" field whenever

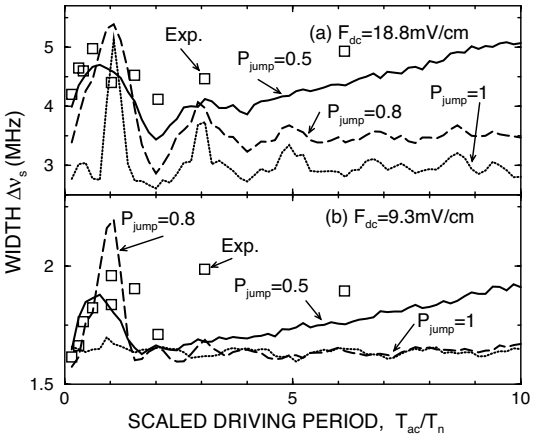

FIG. 5. Width $\Delta\nu_s$ of the peak at the Stark frequency $\nu_s=3nF_{dc}/(2\pi)$ in the Fourier transforms of the survival probability for (a) $F_{dc}=18.8$ mV/cm and $\Delta p_{probe}=-0.532/n$ a.u. and (b) $F_{dc}=9.3$ mV/cm and $\Delta p_{probe}=-0.693/n$ a.u. In (b) the measured width is multiplied by 0.7 (see text). In both cases $\Delta F=0.1F_{dc}$.

the electron orbital frequency ν_n^0 approximately matches the driving frequency ν_{ac} or its higher odd harmonics. This resonant excitation broadens the n-distribution leading to an enhanced $\Delta\nu_s$ seen in Fig. 5. With decreasing P_{jump}, the driving becomes more random (i.e., noisy), and its spectral density broadens, its peak shifting towards lower frequencies (see Fig. 1). Thus, the peaks at the resonant frequencies seen in Fig. 5 become broader and their centers are slightly shifted. CTMC simulations for random noise ($P_{jump}=0.5$) reproduce well the measured results. (A correction factor 0.7 is applied to the measured data for $F_{dc}=9.3$ mV/cm to compensate for the differences caused by the Fourier transformation of data sets with different time resolutions.) The calculations in Fig. 5 show that with increasing T_{ac} the peaks in Fig. 5 not only become broader but, in fact, split into two peaks (clearly seen for periodic driving). This splitting is directly related to the splitting observed in Fig. 3 near the Kepler frequency ν_n^0. Accordingly, the split peaks in Fig. 5 occur when the high harmonics of the noise frequency $(2j+1)\nu_{ac}$ resonantly match the frequencies $\nu_n(-n)=\nu_n^0-\nu_s/2$ or $\nu_n(n)=\nu_n^0+\nu_s/2$. Therefore, the condition (17) is better described as $T_{ac}\nu_n(\pm n)=2j+1$.

Because the Stark frequencies depend on the principal action n of the system, as $\nu_s=3nF_{dc}/(2\pi)$, the growth of $\Delta\nu_s$ is directly related to a broadening of the n distribution, or equivalently, of the energy distribution, associated with the wave packet. As illustrated in Fig. 6, the energy distribution shows a strong broadening for the resonant frequency $T_{ac}=2T_{ran}=T_n$ and only a slight broadening at $T_{ac}=4T_{ran}=2T_n$. Since H_{at} is not constant without noise, the density is plotted as a function of the Stark energy

$$H_{Stark}^{dc} = H_{at} + F_{dc}z = \overline{H_{Stark}^{\eta}(t)}$$
$$= \lim_{N\to\infty}\frac{1}{N}\sum_{\eta=1}^{N}\{H_{at}+[F_{dc}+F_{ran}^{\eta}(t)]z\}. \tag{18}$$

Figure 7 shows that the dependence of the broadening of the energy distribution on the driving period T_{ac} can be un-

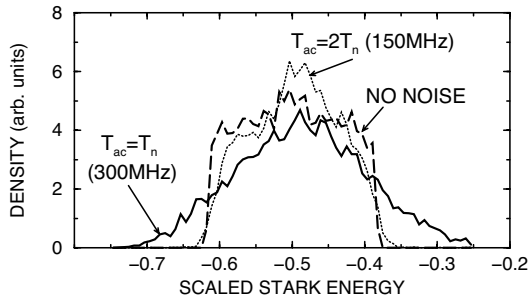

FIG. 6. Calculated scaled Stark energy, $n^2H^{dc}_{\mathrm{Stark}}=n^2(H_{\mathrm{at}}+F_{\mathrm{dc}}z)$, distributions without noise (dashed line) and with $\Delta F=0.1F_{\mathrm{dc}}$ and $F_{\mathrm{dc}}=18.8$ mV/cm for $\nu_{\mathrm{ran}}=300$ MHz (solid line) and $\nu_{\mathrm{ran}}=150$ MHz (dotted line). The distributions are calculated after a time evolution period of 600 ns.

derstood by analyzing the evolution of single trajectories subject to a periodic driving field ($P_{\mathrm{jump}}=1$). Since the Stark energy $H_{\mathrm{Stark}}(t)=H_{\mathrm{at}}+(F_{\mathrm{dc}}+F_j)z$ is a constant of motion between jumps of F_j, excitation can only take place at the jump times $t_j=jT_{\mathrm{ran}}$ when the amplitude of the applied field is switched from $F_{\mathrm{dc}}-\Delta F$ to $F_{\mathrm{dc}}+\Delta F$ (or vice versa). The energy transfer induced by this switch is

$$\Delta H_{\mathrm{Stark}} = \pm 2z_j\Delta F, \tag{19}$$

where z_j is the z coordinate of the electron at $t=jT_{\mathrm{ran}}$. The energy transfer, averaged over the Kepler orbital period $T_n=2\pi n^3$, can be written as

$$\langle\Delta H_{\mathrm{Stark}}\rangle = 2\Delta F(\langle z_j\rangle - \langle z_{j+1}\rangle). \tag{20}$$

Using the fact that z oscillates in time with an orbital period T_n, we can simply approximate $z(t)$ by the dominant frequency component $z(t)=\bar{z}+z_a\sin(2\pi t/T_n)$ to analyze the growth of the energy transfer. At the jump time $t=jT_{\mathrm{ran}}$,

$$z_j = \bar{z} + z_a\sin\left(2\pi j\frac{T_{\mathrm{ran}}}{T_n}\right). \tag{21}$$

In Eq. (20), the constant term $\bar{z}$ is canceled out. Therefore, the energy growth is decided by the interplay of two periodic functions, $z(t)-\bar{z}$ and $F_{\mathrm{ran}}(t)$. When $T_{\mathrm{ran}}\ll T_n$, the oscillation of z_j is so fast that the two terms $\langle z_j\rangle$ and $\langle z_{j+1}\rangle$ cancel each other [Fig. 7(d)] and consequently $\langle\Delta H_{\mathrm{Stark}}\rangle$ and $\langle\Delta n\rangle$ become small [Fig. 7(a)]. However, for $T_{\mathrm{ran}}=T_n/2$ or $T_{\mathrm{ac}}=T_n$, $z_j\sim z_a\sin(\pi j)$ interferes constructively with $F_{\mathrm{ran}}(t)$ [Fig. 7(e)] leading to monotonic changes in the energy $\langle\Delta H_{\mathrm{Stark}}\rangle=2z_a\Delta F$ [Fig. 7(b)]. However, the periodic oscillation of $z(t)$ is also influenced by the Stark precession [see Fig. 7(e)]. After half a period of Stark precession, the orbital phase has been shifted such that the growth in $\Delta H_{\mathrm{Stark}}$ is reversed [Fig. 7(b)]. The growth in width $\langle\Delta\nu_s\rangle$ is, therefore, limited for periodic ($P_{\mathrm{jump}}=1$) but not for stochastic ($P_{\mathrm{jump}}<1$) driving. In contrast, for $T_{\mathrm{ran}}=T_n$ or $T_{\mathrm{ac}}=2T_n$, $z_j\sim z_a\sin(2\pi j)$ interferes with $F_{\mathrm{ran}}(t)$ destructively [Fig. 7(f)] yielding $\langle\Delta H_{\mathrm{Stark}}\rangle\sim 0$ [Fig. 7(c)]. Constructive interference can again be obtained by further increasing T_{ac} and fulfilling Eq. (17). In turn, destructive interference occurs for $T_{\mathrm{ac}}/T_n=2j$.

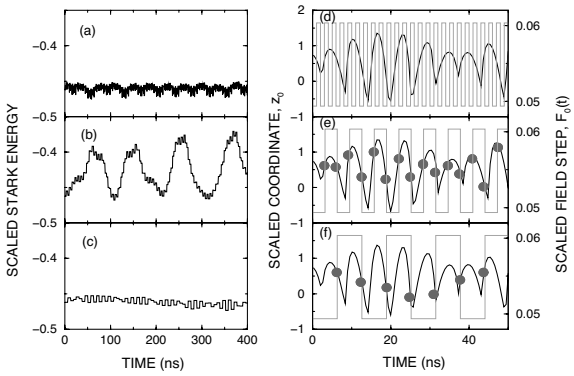

FIG. 7. Time evolution of the scaled Stark energy, $n^2H_{\mathrm{Stark}}=n^2\{H_{at}+[F_{\mathrm{dc}}+F^{\eta}_{\mathrm{ran}}(t)]z\}$, for a single trajectory for (a) $\nu_{\mathrm{ran}}=1$ GHz ($T_{\mathrm{ac}}\ll T_n$), (b) $\nu_{\mathrm{ran}}=300$ MHz($T_{\mathrm{ac}}=T_n$), (c) $\nu_{\mathrm{ran}}=150$ MHz ($T_{\mathrm{ac}}=2T_n$). In (d)–(f) the the scaled electron coordinate $z_0=z/n^2$ is plotted together with the scaled field step $F_0(t)=F(t)n^4$ associated with the periodic driving field. Filled circles in (e) and (f) indicate the electron z-coordinate at the times $t=jT_{\mathrm{ran}}$ (see text for more details). For all cases, $F_{\mathrm{dc}}=18.8$ mV/cm and $\Delta F=0.1F_{\mathrm{dc}}$.

Another remarkable feature of Fig. 5 is that the most prominent peak in $\langle\Delta\nu_s\rangle$ near $T_{\mathrm{ac}}/T_n=1$ depends on P_{jump} non-monotonically. Specifically, for $F_{\mathrm{dc}}=18.8$ mV/cm [Fig. 5(a)], the peak decreases and becomes broader as P_{jump} is reduced from the fully deterministic ($P_{\mathrm{jump}}=1$) to the fully stochastic limit ($P_{\mathrm{jump}}=0.5$), in line with the behavior of $I(\nu=\nu_n^0)$. In turn, for $F_{\mathrm{dc}}=9.3$ mV/cm, the peak is largest for an intermediate level of stochasticity ($P_{\mathrm{jump}}=0.8$). This observation suggests that the absolute amplitude of the noise, ΔF, in addition to its frequency, plays a significant role. Figure 8 displays $\langle\Delta\nu_s\rangle$ as a function of $\Delta F/F_{\mathrm{dc}}$ for two differ-

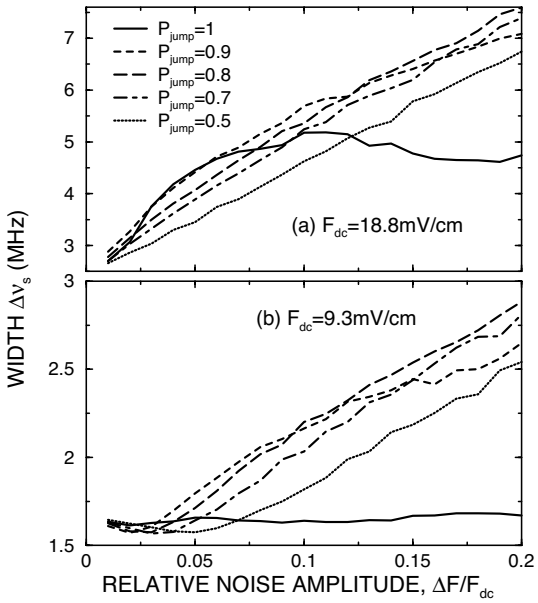

FIG. 8. Width $\Delta\nu_s$ of the peak at the Stark frequency $\nu_s=3nF_{\mathrm{dc}}/(2\pi)$ in the Fourier transform as a function of the noise amplitude ΔF. T_{ran} is set to $T_n/2\simeq 3.26$ ns ($\nu_{ran}=306$ MHz). (a) $F_{\mathrm{dc}}=18.8$ mV/cm and $\Delta p_{\mathrm{probe}}=-0.532/n$ a.u. and (b) $F_{\mathrm{dc}}=9.3$ mV/cm and $\Delta p_{\mathrm{probe}}=-0.693/n$ a.u.

ent field strengths F_{dc}. An approximately linear increase of the damping rate, $\langle \Delta \nu_s \rangle \sim \Delta F$, is observed for $P_{jump} \neq 1$, which is expected for diffusive processes. The case of deterministic driving ($P_{jump}=1$) is exceptional in that $\langle \Delta \nu_s \rangle$ saturates. This result resembles the fact that periodic driving results in trapping inside stable islands, which suppresses further growth in $\langle \Delta n \rangle$ and thus $\langle \nu_s \rangle$. For fixed $\Delta F/F_{dc}$, $\langle \Delta \nu_s \rangle$ decreases with P_{jump}. This is as a direct consequence of the decrease in the spectral density of $I(\nu)$ (the power spectrum of noise in Fig. 1) near $\nu=\nu_n^0$ as a function of P_{jump}.

VI. CONCLUSIONS

We have employed colored noise (generated by randomly modulating the amplitude of a static field at fixed time intervals T_{ran}) to analyze the irreversible dephasing of Stark wavepackets. For "periodic 'noise' " (i.e., periodic driving), when $T_{ac}=2T_{ran}$ is equal to an odd integer multiple of the Kepler orbital period (or, more precisely, of the Stark shifted periods), the electron shows resonant excitation or deexcitation depending on the relative phase of the noise signal and the Kepler motion. As the randomness of the noise increases, the resonant structure is broadened and shifted in frequency depending on the change of the color (and thus the characteristic frequency spectrum) of the noise. Resonant excitation (deexcitation) is especially prominent at $T_{ac}=2T_{ran}=T_n$ where classical coherence is most efficiently destroyed, i.e., the ensemble of classical periodic motion suffers a loss of phase coherence. In contrast, when $T_{ran}=T_n$ statistical coherence survives for much longer periods. The question of noise destroying true quantum coherence, i.e., full or fractional revivals, is also of interest. For Rydberg states with $n=350$ the quantum effects will be difficult to resolve. However, this problem might be addressed through a study of lower Rydberg states. Although attention is focused here on the damping of Stark beats, the role of noise on the damping of the higher-frequency Kepler beats merits further study.

ACKNOWLEDGMENTS

This research is supported by the FWF-SFB-F016 (Austria), OBES, U.S. Department of Energy to ORNL managed by the UT-Batelle LLC under Contract DE-AC05-00OR22725, the NSF (PHY-0353424) and the Robert A. Welch Foundation. J.C.L. acknowledges support from the ONR.

[1] J. A. Yeazell and C. R. Stroud Jr., Phys. Rev. Lett. **60**, 1494 (1988).
[2] A. ten Wolde, L. D. Noordam, A. Lagendijk, and H. B. van Linden van den Heuvell, Phys. Rev. A **40**, 485 (1989).
[3] R. R. Jones, Phys. Rev. Lett. **76**, 3927 (1996).
[4] C. O. Reinhold, J. Burgdörfer, M. T. Frey, and F. B. Dunning, Phys. Rev. A **54**, R33 (1996).
[5] M. Kalinski and J. H. Eberly, Opt. Express **1**, 216 (1997).
[6] H. Wen, C. Rangan, and P. H. Bucksbaum, Phys. Rev. A **68**, 053405 (2003).
[7] H. Maeda, D. V. L. Norum, and T. F. Gallagher, Science **307**, 1757 (2005).
[8] S. Yoshida, C. O. Reinhold, E. Persson, J. Burgdörfer, and F. B. Dunning, J. Phys. B **38**, S209 (2005).
[9] J. Ahn, T. C. Weinacht, and P. H. Bucksbaum, Science **287**, 463 (2000).
[10] M. D. Lukin, M. Fleischhauer, R. Cote, L. M. Duan, D. Jaksch, J. I. Cirac, and P. Zoller, Phys. Rev. Lett. **87**, 037901 (2001).
[11] D. J. Tannor and S. A. Rice, J. Chem. Phys. **83**, 5013 (1985).
[12] W. H. Zurek and J. P. Paz, Physica D **83**, 300 (1995).
[13] K. Hornberger, S. Uttenthaler, B. Brezger, L. Hackermuller, M. Arndt, and A. Zeilinger, Phys. Rev. Lett. **90**, 160401 (2003).
[14] G. C. Ghirardi, A. Rimini, and T. Weber, Phys. Rev. D **34**, 470 (1986).
[15] M. O. Scully, B.-G. Englert, and H. Walther, Nature (London) **351**, 111 (1991).
[16] T. Wellens, V. Shatokhin, and A. Buchleitner, Rep. Prog. Phys. **67**, 45 (2004).
[17] R. Blümel, R. Graham, L. Sirko, U. Smilansky, H. Walther, and K. Yamada, Phys. Rev. Lett. **62**, 341 (1989).
[18] M. Arndt, A. Buchleitner, R. N. Mantegna, and H. Walther, Phys. Rev. Lett. **67**, 2435 (1991).
[19] J. A. Yeazell, M. Mallalieu, and C. R. Stroud Jr., Phys. Rev. Lett. **64**, 2007 (1990).
[20] Z. D. Gaeta and C. R. Stroud Jr., Phys. Rev. A **42**, 6308 (1990).
[21] R. Bluhm, V. A. Kostelecky, and B. Tudose, Phys. Rev. A **55**, 819 (1997).
[22] H. Wen, S. N. Pisharody, J. M. Murray, and P. H. Bucksbaum, Phys. Rev. A **71**, 013407 (2005).
[23] M. T. Frey, F. B. Dunning, C. O. Reinhold, and J. Burgdörfer, Phys. Rev. A **55**, R865 (1997).
[24] C. Raman, T. C. Weinacht, and P. H. Bucksbaum, Phys. Rev. A **55**, R3995 (1997).
[25] H. A. Bethe and E. E. Salpeter, in *Quantum Mechanics of One- and Two-Electron Atoms* (Plenum, New York, 1977).
[26] E. Schrödinger, Naturwiss. **14**, 664 (1926).
[27] R. J. Glauber, Phys. Rev. Lett. **10**, 84 (1963).
[28] Y. Zhang, M. Ciocca, L.-W. He, C. E. Burkhardt, and J. J. Leventhal, Phys. Rev. A **50**, 4608 (1994).
[29] M. Born, in *The Mechanics of the Atom* (G. Bell and Sons, London, 1927).
[30] A. de Kertanguy, I. C. Percival, and D. Richards, J. Phys. B **14**, 641 (1981).
[31] T. P. Hezel, C. E. Burkhardt, M. Ciocca, and J. J. Leventhal, Am. J. Phys. **60**, 324 (1992).
[32] M. T. Frey, X. Ling, B. G. Lindsay, K. A. Smith, and F. B. Dunning, Rev. Sci. Instrum. **64**, 3649 (1993).